PAN
ARCHIVES OF ACOUSTICS
Vol. **45**, No. 3, pp. 521–540 (2020)
DOI: 10.24425/aoa.2020.134069

CC BY SA

Research Paper

Fault Analysis of Worm Gear Box Using Symlets Wavelet

Narendiranath Babu THAMBA[(1)*], Kiran Kamesh THATIKONDA VENKATA[(1)]
Sathvik NUTAKKI[(1)], Rama Prabha DURAISWAMY[(2)], Noor MOHAMMED[(3)]
Razia Sultana WAHAB[(2)], Ramalinga Viswanathan MANGALARAJA[4)]
Ajay Vannan MANIVANNAN[(1)]

[(1)] *School of Mechanical Engineering, Vellore Institute of Technology*
Vellore, Tamil Nadu, India
*Corresponding Author e-mail: narendiranathbabu.t@vit.ac.in

[(2)] *School of Electrical Engineering, Vellore Institute of Technology*
Vellore, Tamil Nadu, India

[(3)] *School of Electronics Engineering, Vellore Institute of Technology*
Vellore, Tamil Nadu, India

[(4)] *Advanced Ceramics and Nanotechnology Laboratory,*
Department of Materials Engineering, University of Concepcion
Chile

(*received April 4, 2019; accepted February 28, 2020*)

This research highlights the vibration analysis on worm gears at various conditions of oil using the experimental set up. An experimental rig was developed to facilitate the collection of the vibration signals which consisted of a worm gear box coupled to an AC motor. The four faults were induced in the gear box and the vibration data were collected under full, half and quarter oil conditions. An accelerometer was used to collect the signals and for further analysis of the vibration signals, MATLAB software was used to process the data. Symlet wavelet transform was applied to the raw FFT to compare the features of the data. ANN was implemented to classify various faults and the accuracy is 93.3%.

Keywords: worm gear box; FFT; symlet wavelets; artificial neural network.

1. Introduction

Worm gear box is found in many applications such as elevators and conveyor belts. The various defects like tooth breakage, pitting and wear, etc. are exerted by worm gear box under varying load condition. It tends to decrease the efficiency of the gear box and in turn leads to decrease in the productivity of the firm. Thus, to find an optimal solution a proposed method is suggested to detect the faults at early stages and to avoid accidents in the future. Therefore, this paper focuses on the vibrational aspects of the worm gear box.

Kalkat (2015) investigated the effect on gearboxes due to the changes in the oil quality using neural network. Five different oil types were used to classify the faults in the gear box using MNN and RBNN. The author proved that RBNN is more predictive than MNN and identified the best oil suited for real time applications.

Peng and Kessissoglou (2003) discussed the correlation of vibration analysis and wear debris analysis. An experimental test rig consisting of a worm gear mechanism and an electric motor was used. Authors tested the gear box along with contaminant particles in the lubricant and normal lubricant. The vibration analysis method gave quick and reliable information on the gear.

Elforjani *et al.* (2012) examined an oil jet sprayed worm gearbox, driven by a reverse variable speed geared motor unit. Tests were done by deforming the gear to simulate real time wear and damage conditions. The paper demonstrates the applicability of acoustic emission technology in detecting defects in worm gear system. Further research proved that Acoustic Emis-

sion (AE) technology is superior to vibration analysis which is widely used technique in fault analysis of gear systems.

Zhang and Wang (2014) described the fault analysis on wind mill gear using ANN. The authors proposed a fault detection method for main bearing wind turbine based on existing SCADA data using an artificial neural network (ANN). The results show that ANN handles a large volume of SCADA data and provide information about wear.

Fan and Zuo (2006) investigated gear box fault detection, and in their studies demodulation is considered to be an important issue. Demodulation becomes difficult due to the non-stationary modulating signals. Although wavelet packet transform has better time–frequency localization because of the existence of meshing frequencies. The harmonics and coupling frequencies in the fault detection using wavelet packet transform alone are unsatisfactory in a multistage gear box containing close frequency components. A new fault detection method Hilbert transform and wavelet packet transform was proposed in this paper.

Kumar and Singh (2013) investigated the features of the images of the rolling element bearing in rotary machines. Experiments were carried out on a customized experimental setup by seeding various defects on the outer race defect width of taper roller bearing. For feature extraction, the symlet wavelet was used because of its nature which allows to maintain the sharpness of the signal even when there is a sudden change in the signal. The authors' investigation showed the maximum deviation to be as 4.06% for the defect width of 1.1820 mm at no load and decreased further with increase in the load.

Jing *et al.* (2017) investigated and presented convolutional neural network, feature learning and fault diagnosis method for condition monitoring of gear box using processed data. Continuous wavelet transform was used for fault diagnosis of gear box by using vibrational signals and artificial neural networks. The classification algorithm was developed and provided 98% efficiency.

Singh and Parey (2019) investigated the independent angular re sampling technique which was utilized to convert the non-stationary vibration and sound signals to quasi-stationary signals in angular domain. Further, they used a technique called back propagation neural network to classify the faults.

Wang and McFadden (1996) investigated and found out the definition of wavelet transform and then showed how it could be utilized for the analysis of vibrational signals produced by a gear in the helicopter gear box. They showed that unlike the conventional time-frequency distribution which uses constant time resolution, the wavelet transform can display simultaneously both large and small sizes in the signal.

Elasha *et al.* (2014) investigated the condition of three different worm gearboxes. Conditions were assessed using various vibration signal analysis techniques which included a few statistical measures, Spectral Kurtosis and enveloping. This was examined to identify the presence of defects within the worm gearboxes.

Ghodake *et al.* (2016a; 2016b) stated that the wear debris analysis is the main method to detect fault in worm gearbox, after that vibration analysis methods are used to detect faults in worm gearbox. The vibration signal expresses the signature of various fault in the worm gearbox. This vibration signature was analyzed to identify the fault in worm gearbox. The two parameters e.g. time domain and frequency domain analysis were chosen for detection of faults. The authors also reviewed the fault analysis on the worm gear box.

Ismon *et al.* (2015) examined the vibration behaviour of worm gear as function of gear lubricant's viscosity. Three different types of lubricant's viscosity were used in the investigations such as VG100, VG460 and VG680 to serve the sliding friction of worm gears. The various speeds of electric motor at 900 rpm, 1150 rpm, and 1400 rpm were introduced to the gearbox to measure the vibration signal and temperature profile.

Tilak and Krishnakumar (2015) examined the effectiveness of symlets in de-noising fingerprint images. The effectiveness of de-noising with each member of the selected set of members of the symlet wavelet family was examined with the standard performance measures, namely the Mean Squared Error, along with the seeming visual quality of the de-noised image.

2. Experimentation

2.1. Experimental setup

It was decided to induce faults like tooth breakage and some other faults to the wheel in the gear box. The analysis of every vibration was carried out separately. In the worm gear box the worm wheel was made up of BS1400 PB2C bronze alloy. The worm screw was made out of EN34 steel. The gear box chosen for the experimentation was of 50 :1 gear reduction ratio and the DC motor used is of ½ HP and 1440 rpm. The gear box and the motor were coupled using a V-type belt with a determined offset that delivers the required rpm to the input shaft of the gear box. The entire setup was mounted on a wooden bed to dampen the unnecessary vibrations and also the wooden bed was provided with plastic bushes to reduce the vibrations. To eliminate the shock from the motor, rubber pads were provided under both the motor and the gear box. Finally, a magnetic accelerometer with 100 m/g sensitivity used to collect the vibration was placed on the gear box at a point at which it could give better signals.

2.2. Experimental procedure

This study was carried out to recognise the behaviour of worm gear box at different conditions. The experiments were performed for 3 oil conditions, i.e. full oil, half oil and quarter oil conditions without any load. The speed was kept constant at 1440 rpm. Experimentation was carried for healthy gear box along with 4 different faults with the above mentioned 3 oil conditions at 1440 rpm. Figure 1 shows experimental set up1 including data acquisition system. Figure 2 shows the experimental setup 2 including motor, worm gear box and V-belt drive. Table 1 shows summary on the type of faults induced on the gear box.

Fig. 1. Experimental setup 1.

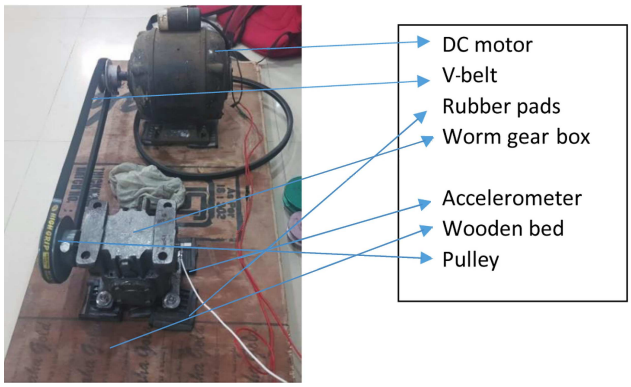

Fig. 2. Experimental setup 2.

Table 1. Summary on the type of faults induced on the gear box.

Fault 1	2 mm length of edge removal of small portion of one tooth shown in Fig. 3
Fault 2	5 mm length of removal of half of the tooth shown in Fig. 4
Fault 3	10 mm length of two teeth removal shown in Fig. 5
Fault 4	3 mm length multiple faults like edge removal of the consecutive tooth shown in Fig. 6

Fig. 3. Fault 1.

Fig. 4. Fault 2.

Fig. 5. Fault 3.

Fig. 6. Fault 4.

In the experimental investigation, the vibration signals were collected at an ideal condition without any crack or wear, i.e. healthy surface at the shaft speed of 1440 rpm. The readings were recorded at a sampling rate of 12 000 Hz. The 621B40 M I accelerometer type, sensor having sensitivity 1.02 mV/m/s^2 and frequency range up to 12 kHz, was used in horizontal position on the bearing housing with magnetic base to collect the vibration data. The other end of the accelerometer was connected to the vibration data collector with DWESOFT software. Finally, MATLAB software was used for various signal processing.

2.3. Methodology

The vibration signals were captured using the magnetic accelerometer in the software Dewesoft and data were exported to excel for further analysis using MATLAB. Both time domain analysis and frequency domain analysis were done to study the nature of the signals. Initial FFT was not suitable for the study because of the noise that was present in the data and for this reason wavelet decomposition was done to cancel out the noise and extract the required frequency and amplitude. The excel data were further utilized for ANN.

2.4. Frequency domain analysis

It helps in decomposing a complex signal into simpler parts to facilitate further analysis. It was done by several differential and difference equations and various convolutional operations in the time domain which become algebraic operations in the frequency domain. This is usually achieved through the application of FFT. The mathematical Eqs (1) and (2) are given below:

$$\text{DFT(FFT)}: \tag{1}$$

$$X(k) = \sum_{n=0}^{N-1} x(n) e^{-j\left(\frac{2\pi}{N}\right)nk}, \qquad k = (0, 1, ..., N-1), \tag{2}$$

where $X(k)$ is in frequency domain and $x(n)$ is in time series domain. MATLAB shall be used to implement FFT on the data collected in experimentation. Threre was an increase in the computing speed of DFT while using the FFT by reducing the number of computations from $2N^2$ to $2N \log 2N$ for N data.

2.5. Wavelet decomposition

The symlets wavelets are not symmetric, instead they have the least amount of asymmetry for a given support. Hence, they are called 'near symmetric wavelets'. In fact they have better symmetry than another family of orthogonal wavelets, i.e. the Daubechies wavelet family. Symmetry of the filter coefficients is needed since symlet results in linear phase of the transfer function. Rajput and Kumar (2015) suggested that the symlet wavelets have unitary lossless functions. This is used to simplify the transform coefficients calculation.

Symlets are wavelets which posses compact support. The symlet wavelet filters are Finite Impulse Response (FIR) filters, therefore the filter values drop to zero outside a finite duration of time. A symlet is referred to as "sym N", where N is the order of the wavelet. Then a symlet has a length of $2N$ for its filter and has a support width of $2N - 1$ (Tilak, Krishnakumar, 2015).

For extracting the feature from the signal, the technique of CWT (Continuous Wavelet Transform) was used in the analysis that decomposed the signal in frequency domain. Mathematically, CWT is expressed in Eq. (3)

$$\text{CWT}(a, b) = \frac{1}{\sqrt{a}} \int_{-\infty}^{\infty} X(t) \Psi^*(t-b)/a \, \mathrm{d}t, \tag{3}$$

where a indicates the scale parameter, b indicates the translation parameter, Ψ represents the mother wavelet and Ψ^* indicates the complex conjugate, the decomposition using the wavelet may consume some time depending on the resolution that we desire. Since CWT lacks in redundancy with digital computers because of taking continuous parameters like (a, b), thus scale and shift parameters are evaluated on a grid that is discrete of time scale plane leading to a set of continuous basis functions. The DWT is a discrete form of CWT. It uses the dyadic scale and translation to reduce the time taken for computation. Symlet wavelets are more symmetrical than the Daubechies wavelets. At some points they even generate a linear phase which makes it easier to deal with small discontinuity present in the signal without major loss of information. Symlets have a perfect reconstruction and cancellation ability that facilitates the use in both CWT and DWT.

The modification of Daubechies wavelets to symlets was done in the following way where the mother wavelet function m_o introduced in the dbN, considering the $|m_o(\omega)|^2$ as a function of $Z = e^i$. Thus, the use of symlet wavelet allows us to recognise the GMF and the peak of vibration in the frequency domain thoroughly.

2.6. Fault classification using ANN

The technique of ANN comes handy when we want to know the health condition of the gear box because it helps in continuous conditional monitoring of the gear box when it runs continuously at different conditions without the intervention of humans. It evaluates parameters like performance, severity of the fault and degree of performance degradation.

Firstly, vibrational data of the healthy gear box running at 1440 rpm at three different oil conditions were extracted for a duration of 60 seconds, then for 10 seconds of the data feature extraction was done to gain knowledge on the performance of the gear box. Similarly the same data extraction method was followed for various faults at different oil conditions and the same feature extraction method was followed for the first 10 seconds of data. The nine time domain features include mean, variance, RMS, median, kurtosis, skewness, standard deviation, peak to peak, crest factor which is shown in Eqs (4)–(12).

$$\overline{X} = \frac{1}{n} \sum_{i=1}^{n} |x_i|, \tag{4}$$

$$X_{\text{median}} = \frac{\frac{n}{2} - cf}{f}(w) + L_m, \tag{5}$$

$$\text{SD} = \sqrt{\frac{\sum |x - \overline{x}|^2}{n}}, \tag{6}$$

$$X_{\text{var}} = \frac{1}{n} \sum_{i=1}^{n} (x_i - \overline{X})^2, \tag{7}$$

$$X_{\text{RMS}} = \sqrt{\frac{1}{n} \sum_{i=1}^{n} x_i^2}, \tag{8}$$

$$X_{\text{kur}} = \frac{1}{n}\frac{\sum_{i=1}^{n} x_i^4}{X_{\text{RMS}}^4}, \tag{9}$$

$$X_P = \frac{1}{n}\sum_{i=1}^{n} X_{pi}, \tag{10}$$

$$X_{cf} = \frac{X_P}{X_{\text{RMS}}}, \tag{11}$$

$$X_{\text{skew}} = E\left[\left(\frac{x-\mu}{\sigma}\right)^3\right]. \tag{12}$$

Taking 6 samples from each of 5 available cases were made a matrix of 30×9, thus this data were separately stored in an excel sheet and modelled using the pattern recognition tool or the npr tool feature in the MATLAB. Therefore, for the analysis we made use of the 9 features as inputs and by default 10 hidden layers. 70% of the data was utilized for training and 15% each for validation and testing the neural network. The overall performance of the ANN was assessed by various plots like error histogram, confusion matrix, cross entropy, ROC, etc.

3. Results and discussion

The vibrational data that had been acquired, was utilized to recognise the features of the gear box at different conditions. Wavelet decomposition using symlets was done for the raw signal data to obtain a filtered FFT. For the current study worm gear box of 50 :1 was used and for validating the data, the features of the signal were compared with GMF (gear mesh frequency). The gear box ran at 1440 rpm and its frequency was rpm/60 = 24 Hz. The number of teeth in contact between worm and worm wheel was 1. Therefore, the gear mesh frequency was the frequency of the contact between the worm wheel and worm gear. It can be calculated by multiplying the rotational frequency of the input gear shaft with the number of teeth

$$\text{GMF} = \text{NT} \times \text{RFIS},$$

where NT – number of teeth, RFIS – rotational frequency of the input shaft.

So, GMF gave the value of 24 Hz and thus, this value was used to validate the data in the power spectrum plot of the worm gear box.

3.1. Worm gear box at healthy condition

3.1.1. Full oil condition

For the ease of feature analysis it was decided to proceed with 4th wavelet at 5th level of the decomposition for all the signals at all the possible conditions because in the fourth and fifth level of wavelet, the maximum amplitude of vibration was observed. Therefore, in this way the raw signal data were decomposed and FFT was plotted for the decomposed data and the signal processing was carried out for the healthy gears. Figure 7a shows symlet decomposition of time domain for full oil healthy condition. Figure 7b shows time domain for full oil healthy condition. The raw signal was collected for 10 seconds at the sampling rate of 12 000 Hz. Then readings were processed with MATLAB software to convert time *versus* amplitude plot. Figure 7c shows FFT raw signal for full oil healthy condition where FFT represents a GMF of 24.81 Hz and a peak amplitude of 0.125 m/s^2. Figure 7d shows symlet decomposed signal through FFT full oil healthy condition, where decomposed FFT represents a better resolution of the vibrations with a GMF of 24.54 Hz and a peak amplitude of 0.001893. It proves that the decomposition was successful since there was a decrease in the peak amplitude and also the GMF 24.54 Hz nearly corresponds to the value 24 Hz.

It is well known that the most important components in gear vibration spectra are the tooth meshing frequency and its harmonics, together with sidebands due to modulation phenomena. The increment in the number and amplitude of such sidebands may indicate a fault condition. It may serve as a tool for aiding the gear fault diagnosis. The GMF and its side bands are represented in various power spectrums with indication of data cursor amplitude value of around 0.0018, and 0.0015 respectively. The GMF and side bands of GMF are depicted in Fig. 7d.

3.1.2. Half oil condition

The same gears were run at a half of the oil level of gear box. Figure 8a shows time domain for half oil condition. Figure 8b shows symlet decomposed signal through FFT for half oil condition. From Fig. 8b, it can be observed that there is an increase in the vibrations since the oil level was reduced to half with a GMF of 24.54 Hz and peak amplitude of 0.001937 m/s^2 indicating the increase in the amplitude of the vibration when compared to that of full oil is 0.001893 m/s^2.

As seen in symlet wavelet based enveloped power spectrums, vibration amplitude at GMF is increasing inline with the severity of fault from low value to high value with dominant sidebands, indicating severity of fault. For a gear box in good condition, side band level remains low as seen in Fig. 7d. The symlet wavelet analysis is powerful in isolating peaks at sidebands of GMF which can provide more precise information about defect condition. Vibration amplitude of side bands is significant. Changes in the number and strength of the side bands indicate severity of fault.

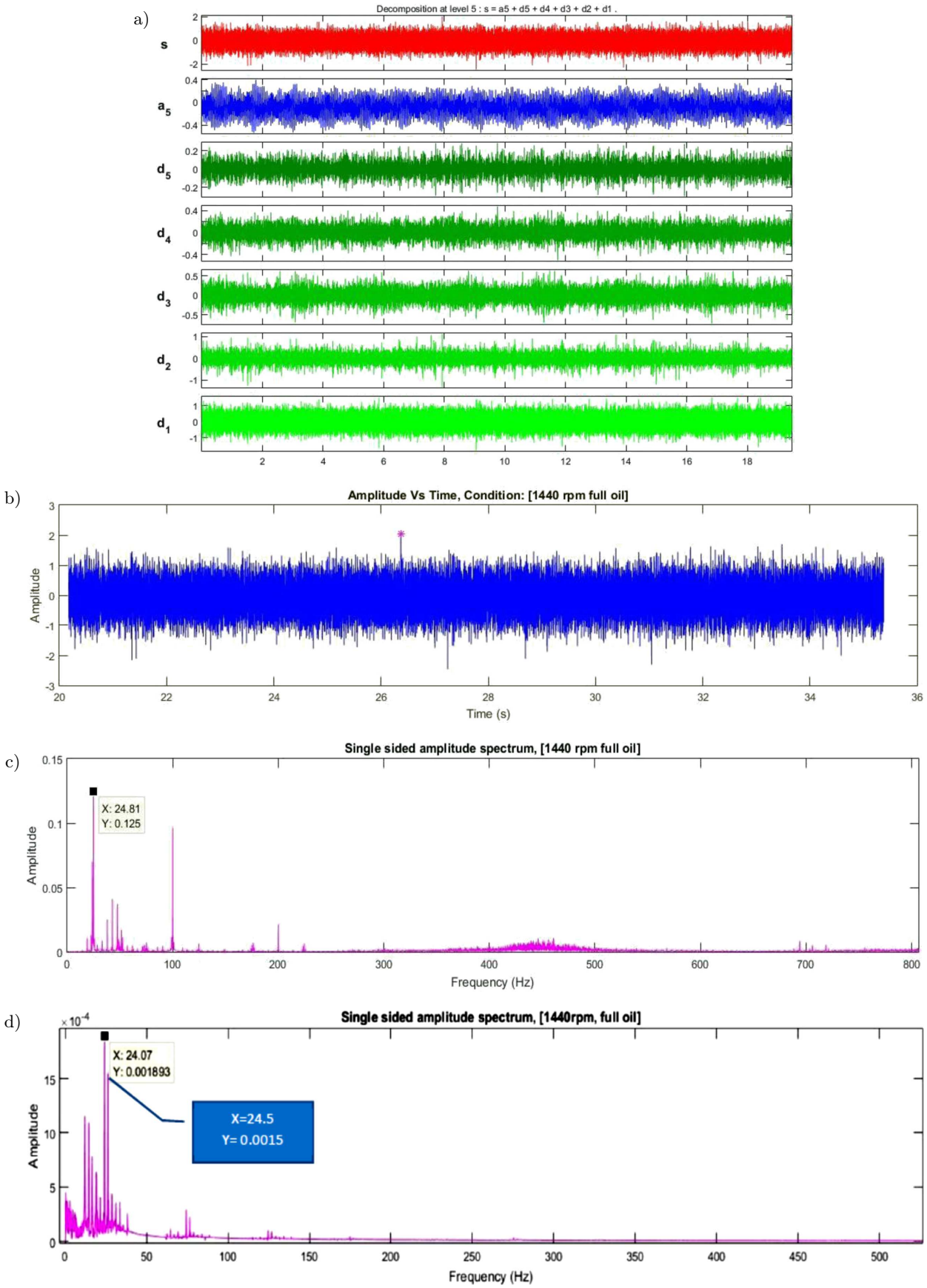

Fig. 7. a) Symlet decomposition of time domain for full oil healthy condition, b) time domain for full oil healthy condition, c) FFT raw signal for full oil healthy condition, d) symlet decomposed signal through FFT full oil healthy condition.

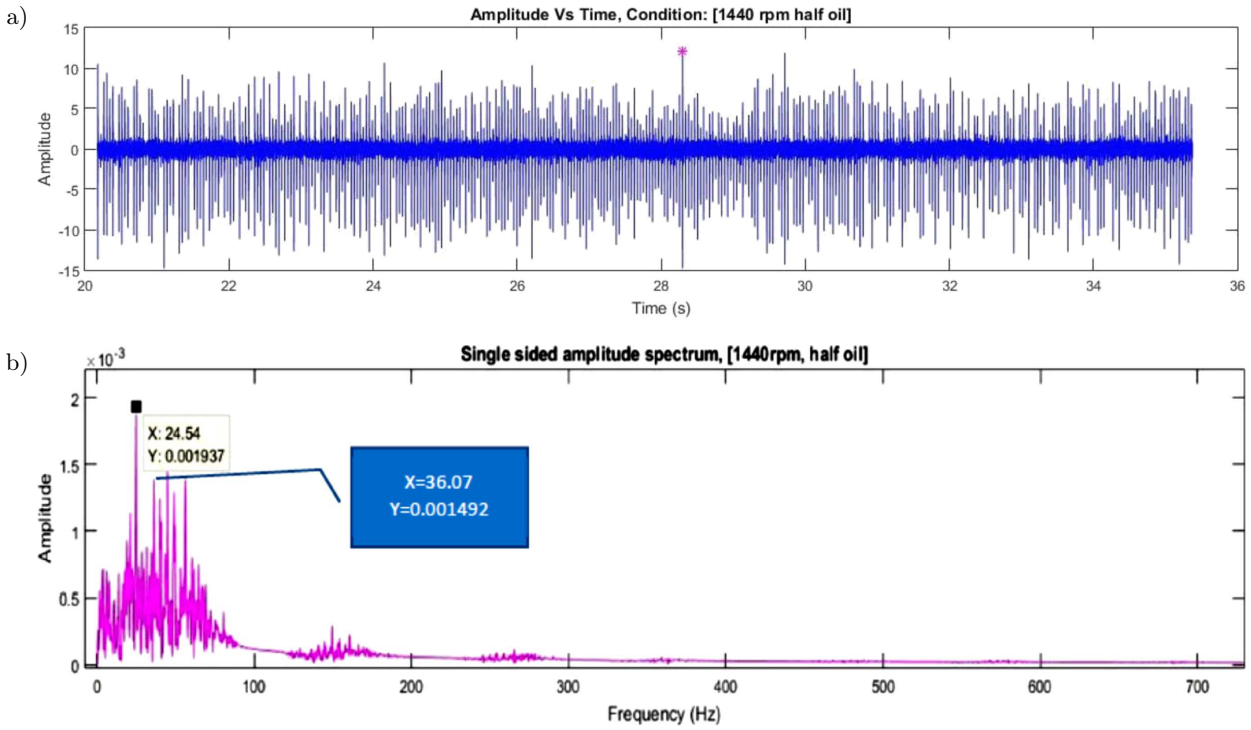

Fig. 8. a) Time domain for half oil condition, b) symlet decomposed signal through FFT for Half oil condition.

3.1.3. Quarter oil condition

After collection of the readings from the gear box containing half oil, further half of the oil was removed through the drain plug from the existing gearbox leaving a quarter of oil in the gear box. Figure 9a shows the time domain signal for a quarter oil condition. Figure 9b shows the symlet decomposed signal

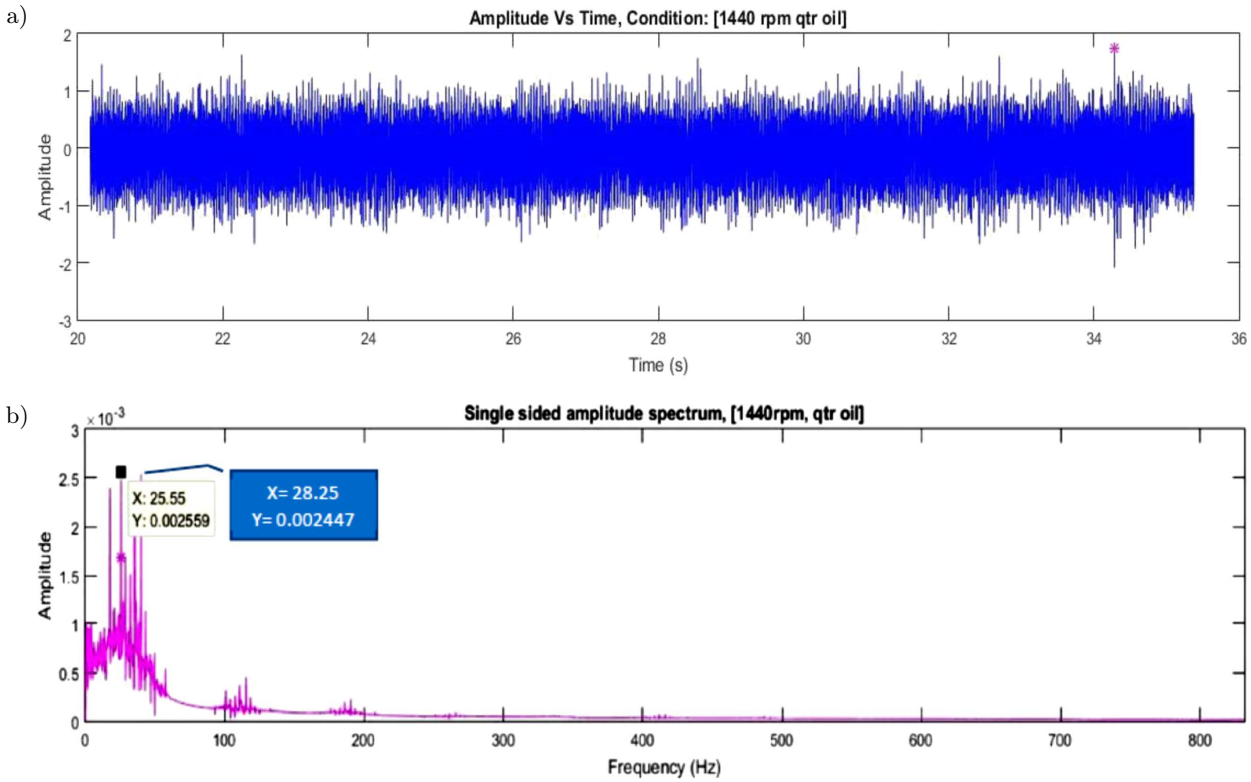

Fig. 9. a) Time domain signal for quarter oil condition, b) symlet decomposed signal through FFT for quarter oil condition.

through FFT for a quarter oil condition. From Fig. 9b it is observed that the GMF starts to fluctuate due to a decrease in the oil level that is from 24.54 Hz to 25.55 Hz and the peak amplitude is bounced to a value of 0.002559 m/s^2. Thus, an increase trend in the amplitude of vibration was noticed in the functioning of gear box at different oil levels.

As seen in symlet wavelet based enveloped power spectrums, vibration amplitude at GMF increases inline with the severity of fault from 0.0015 to 0.0024 value with dominant sidebands, indicating severity of fault.

3.2. Worm gear box with fault 1

Next, a small tooth was removed causing an improper meshing between the worm and the wheel, which resulted in an increase in the amplitude of vibration due to fault.

3.2.1. Full oil condition

For the full oil condition with fault 1, it is noticed that the GMF was unaltered to an extent when compared to that of the quarter oil condition for the healthy gear box 25.59 Hz. Figure 10a shows time domain signal for fault 1 under full oil condition. Figure 10b shows symlet decomposed signal through FFT for fault 1under full oil condition, and the peak amplitude is shown as 0.1212 m/s^2 which illustrates an increase in amplitude due to the presence of fault when compared with values of a healthy gear box. As seen in symlet wavelet based enveloped power spectrums, vibration amplitude at GMF increases inline with the severity of fault from 0.0015 to 0.0937 amplitude value with dominant sidebands, indicating severity of fault.

3.2.2. Half oil condition

Then the half oil condition maintained in the gear box and vibration data were collected at fault 1 condition. Figure 11a shows time domain signal for fault 1 under half oil condition. Figure 11b shows the symlet decomposed signal through FFT for fault 1 under half oil condition. The readings shows that there is an increase in the magnitude of the peak amplitude as 0.1562 m/s^2 with a frequency of 25.35 Hz. As seen in symlet wavelet based enveloped power spectrums, vibration at GMF increases inline with the severity of fault 27.72 Hz with dominant sidebands, indicating severity of fault.

3.2.3. Quarter oil condition

Quarter oil level condition was maintained in the gearbox and the vibration data were collected at fault 1. Figure 12a shows time domain signal for fault 1 under quarter oil condition. Figure 12b shows symlet decomposed signal through FFT for fault 1 under quar-

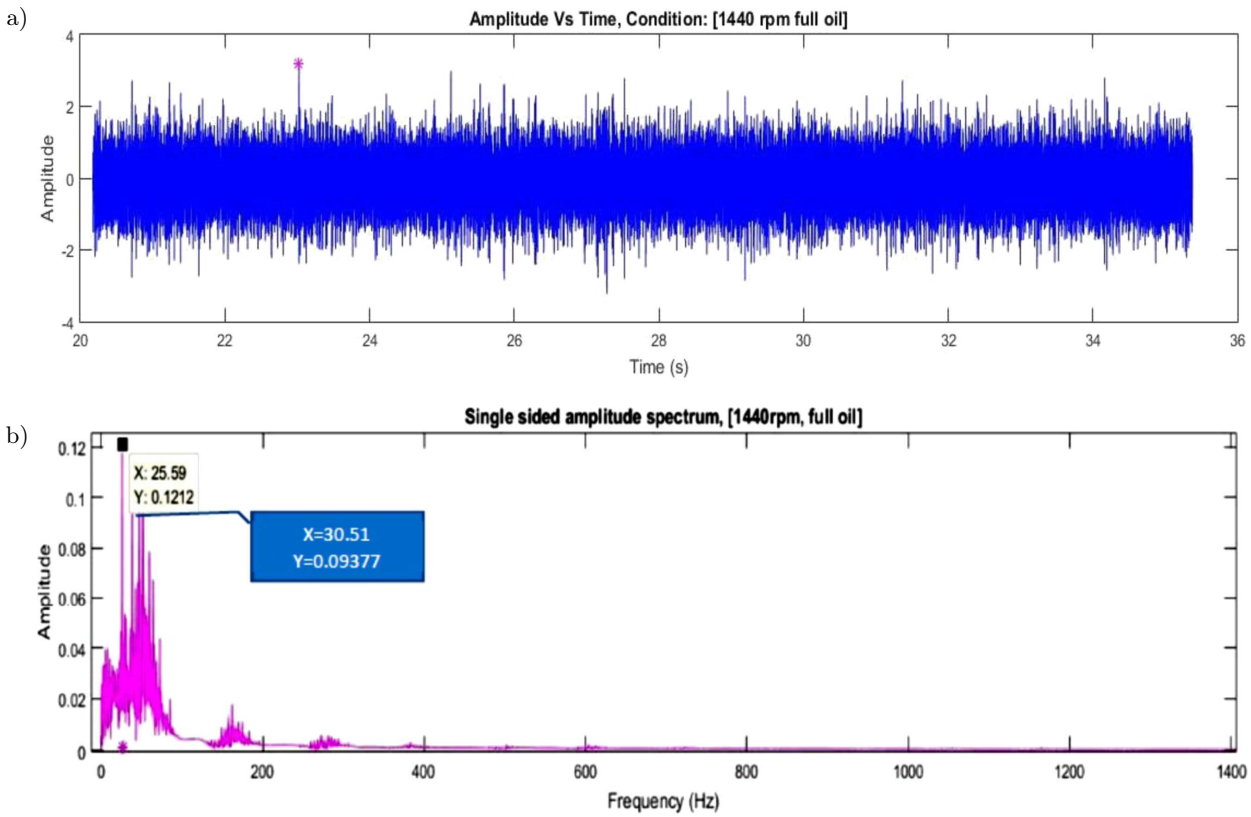

Fig. 10. a) Time domain signal for fault 1 under full oil condition, b) symlet decomposed signal through FFT for fault 1 under full oil condition.

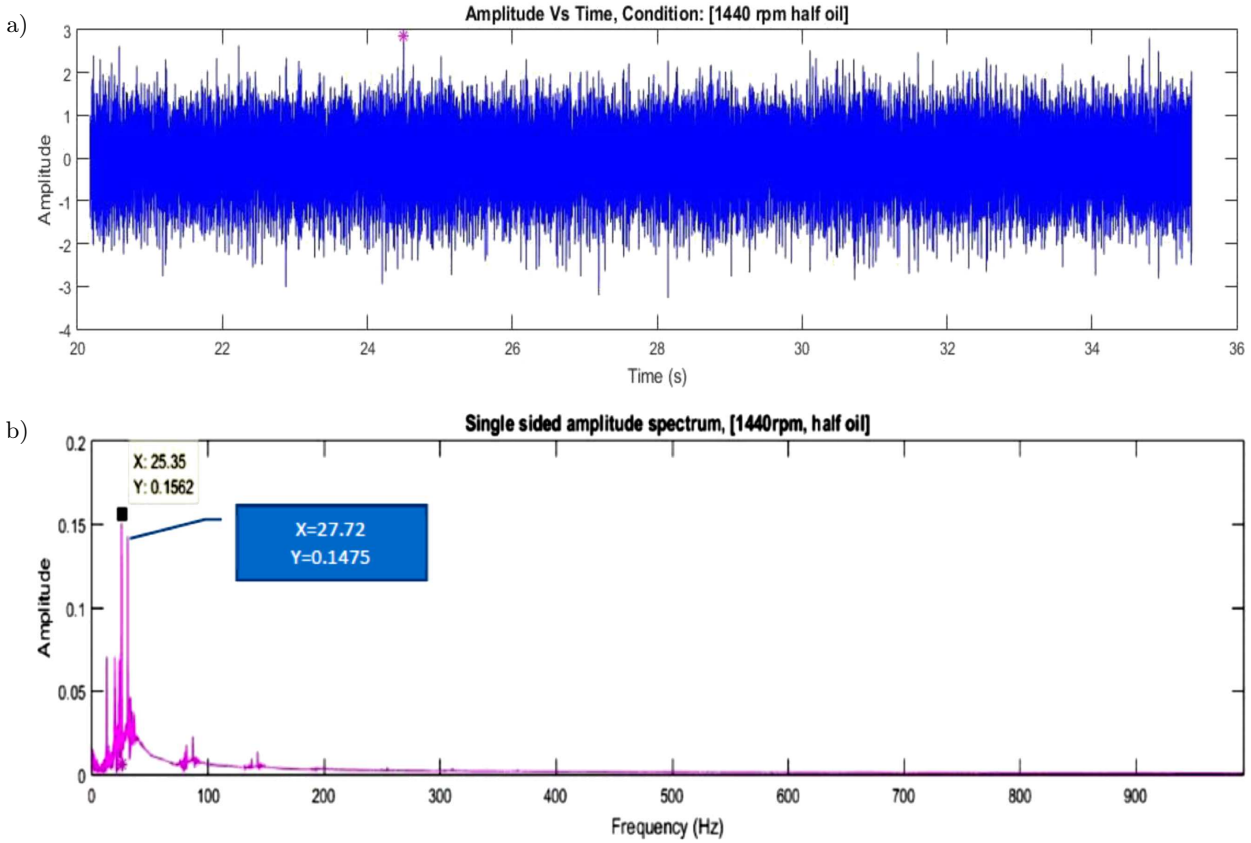

Fig. 11. a) Time domain signal for fault 1 under half oil condition, b) symlet decomposed signal through FFT for fault 1 under half oil condition.

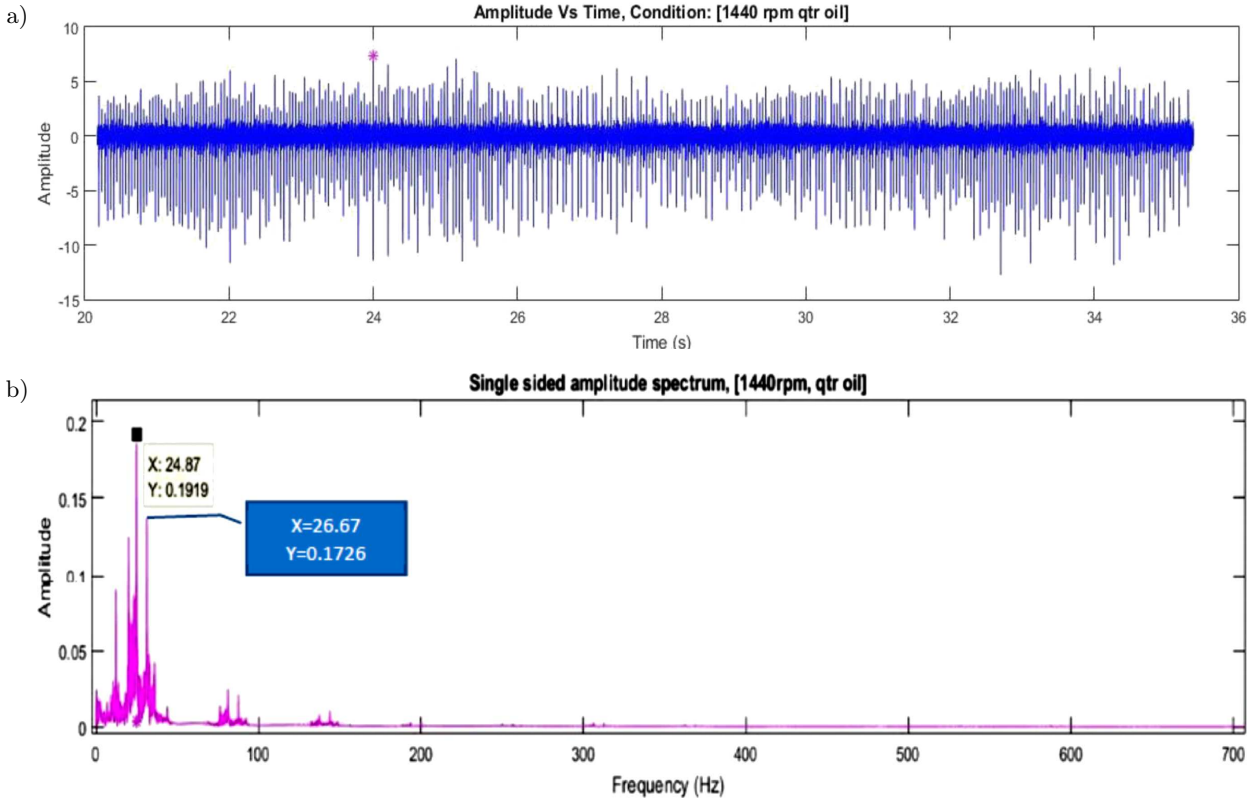

Fig. 12. a) Time domain signal for fault 1 under quarter oil condition, b) symlet decomposed signal through FFT for fault 1 under quarter oil condition.

ter oil condition. Now, the FFT graphs for both the half oil condition and quarter oil condition are almost the same since there is not any significant change in the oil level but it leads to an increase in the amplitude of vibration that is to a value of 0.1919 m/s^2 (Fig. 9f). As seen in symlet wavelet based enveloped power spectrums, vibration amplitude at GMF increases inline with the severity of fault with 26.67 Hz and amplitude value of 1726 with dominant sidebands, indicating severity of fault.

3.3. Worm gear box with fault 2

Fault 2 corresponds the fault where the tooth were removed to half of the extent. Thus, practically as the magnitude of fault increased then the peak amplitude also increased and same was inferred from the plots.

3.3.1. Full oil condition

For the full oil condition there was not a significant amount of vibrations. Fig. 10b shows the GMF is 25.09 Hz and the amplitude is 0.4295 m/s^2. As seen in the symlet wavelet based enveloped power spectrums, vibration amplitude at GMF increases inline with the severity of tooth fault from 0.0018 to 0.4295 mm/s^2 with dominant sidebands, indicating severity of fault. For a gear box in good condition, side band level remains low as seen in Fig. 7d. The symlet wavelet analysis is powerful in isolating peaks at sidebands of GMF which can provide more precise information about defect condition.

3.3.2. Half oil condition

Corresponding to this condition as the amount of oil was reduced to half again there seems to be a significant rise in the vibrations, the GMF is almost the same as at the full oil condition, from Fig. 10d the GMF is 25.23 Hz and the peak of the amplitude was increased to 0.4607 m/s^2.

A large increase in sideband amplitude suggests that something changes in the geometry and is also a cause of concern. The relative amplitude of sideband to gear mesh peak is a good parameter to see in the plot. Scrutinize the waveform for periodic impacts that relate to rotational speed of the gears. Gear failure will permit unexpected shaft displacement thereby upsetting gear engagement. Often, tooth failure precedes gear damage. Increased impacting from deterioration in the transfer of power may excite gear natural frequencies. From Fig. 14b it is observed that the vibration amplitude of side bands is significant. Changes in the number and strength of the side bands indicate severity of fault.

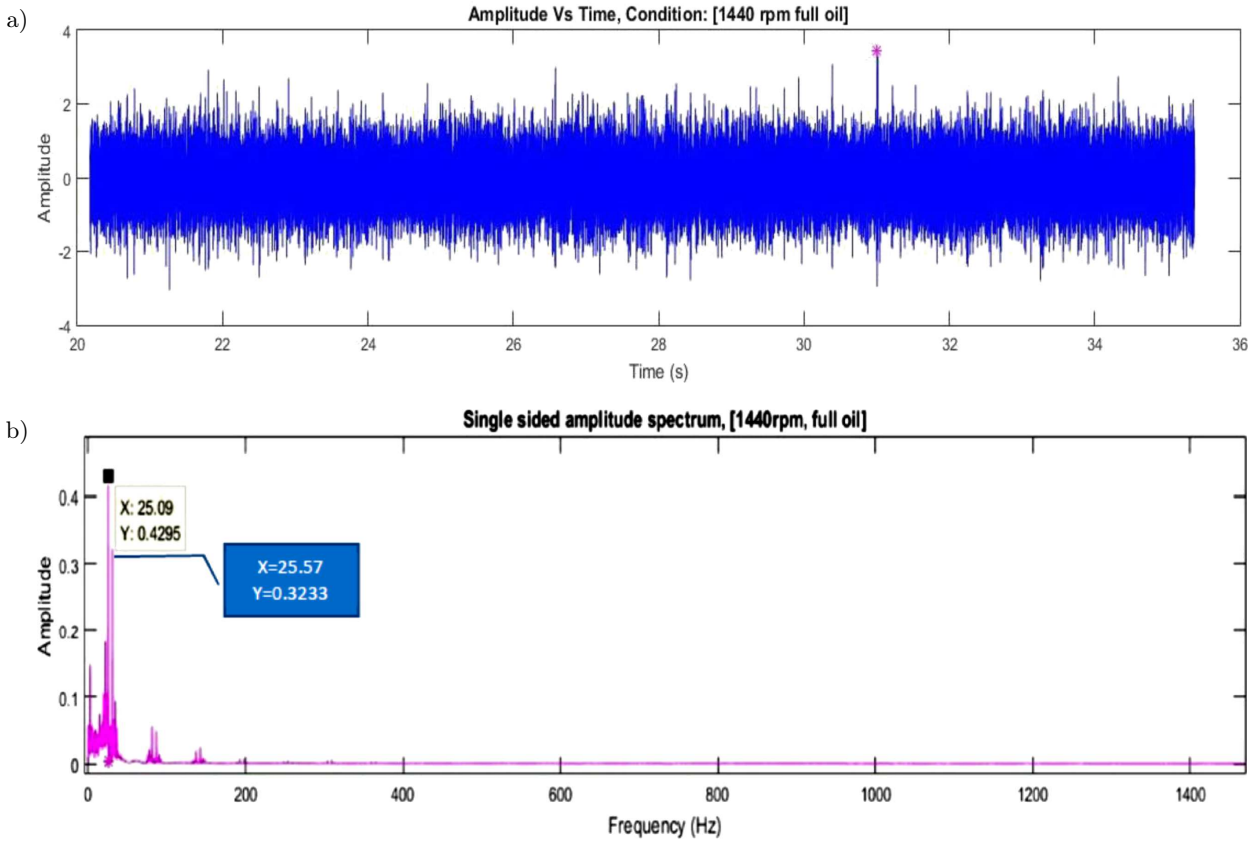

Fig. 13. a) Time domain signal for fault 2 under full oil condition, b) symlet decomposed signal through FFT for fault 2 under full oil condition.

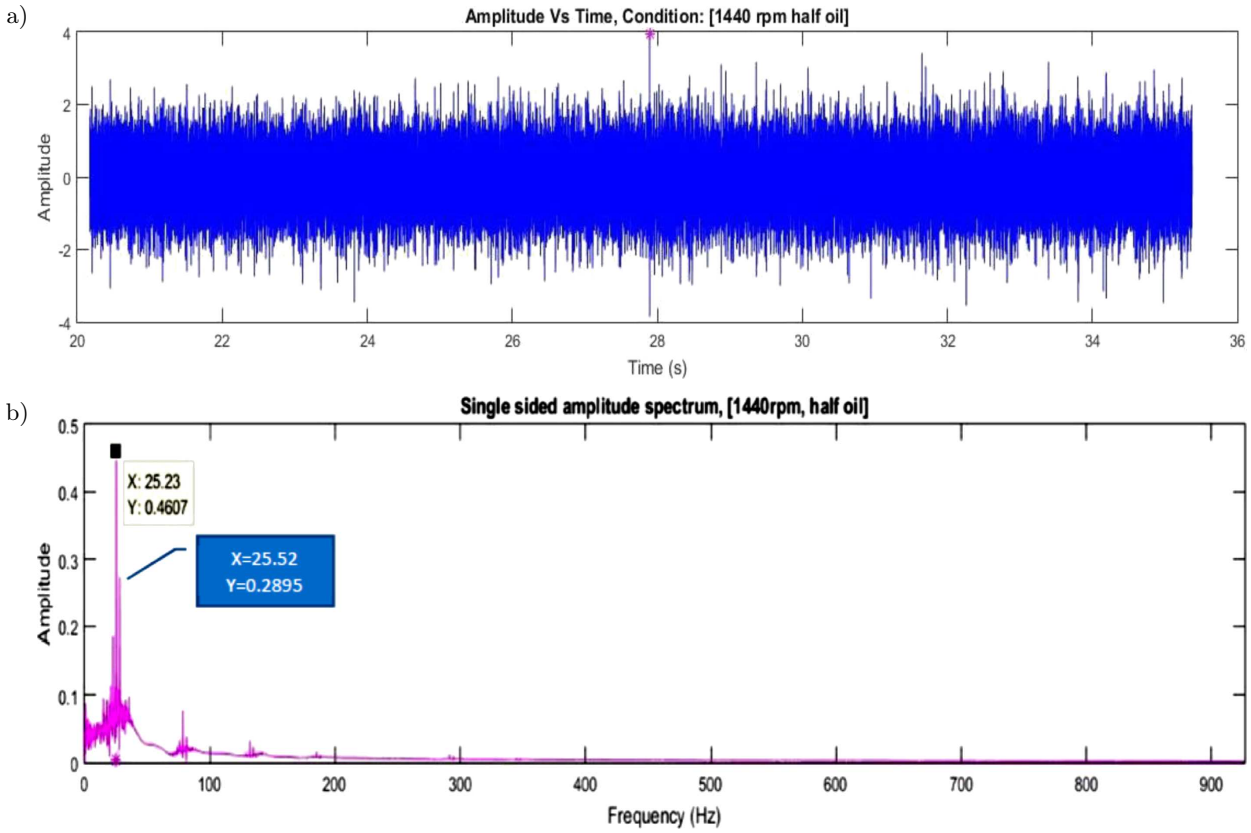

Fig. 14. a) Time domain signal for fault 2 under half oil condition, b) symlet decomposed signal through FFT for fault 2 under half oil condition.

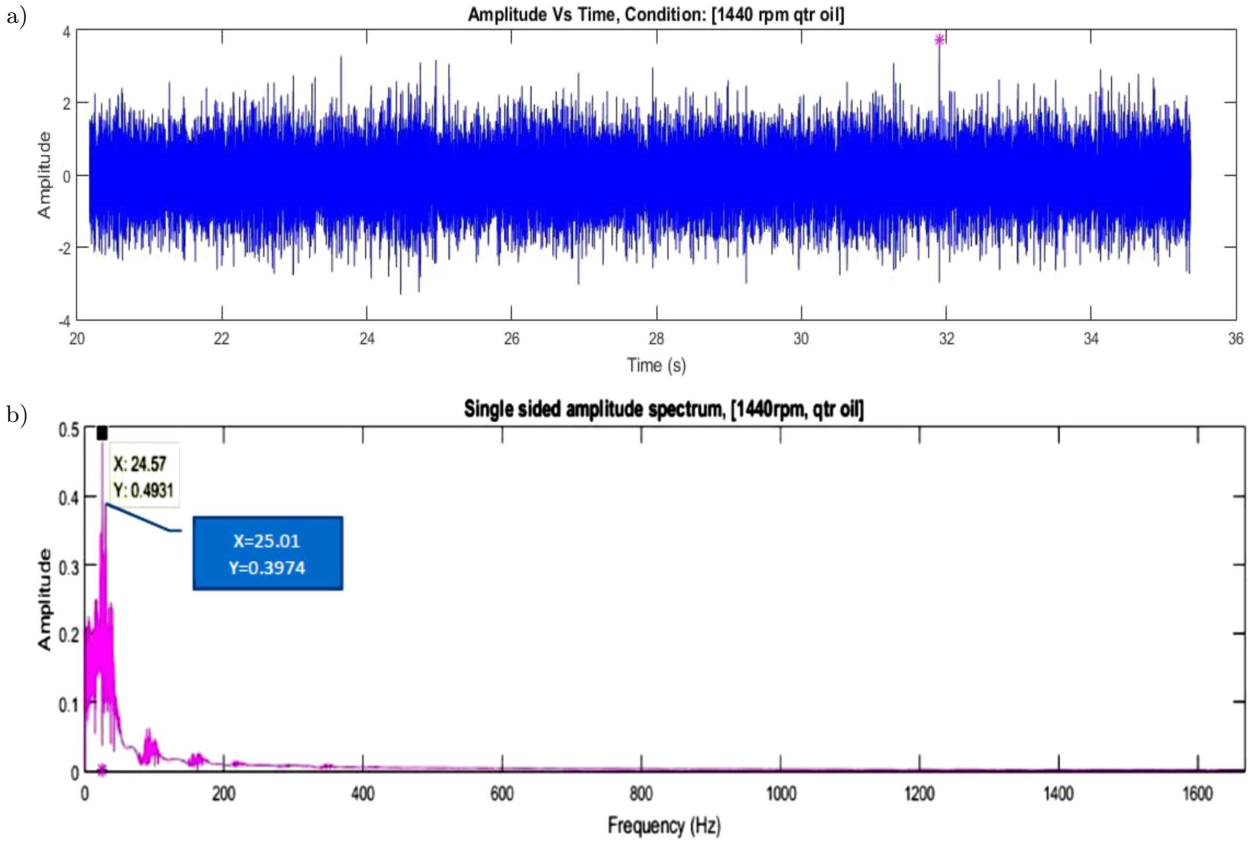

Fig. 15. a) Time domain signal for fault 2 under quarter oil condition, b) symlet decomposed signal through FFT for fault 2 under quarter oil condition.

3.3.3. Quarter oil condition

Corresponding to this condition the amount of vibrations almost remained constant but the GMF and the peak of the amplitude was increased significantly, from Fig. 15b the GMF is 24.57 Hz and the amplitude is 0.4931 m/s^2. The GMF mesh frequency and its harmonics are not expected to be suppressed; thus, the frequency will have the highest amplitude with sidebands around it.

3.4. Worm gear box with fault 3

This fault corresponds to the complete removal of one tooth and the increased magnitude of fault. Due to increased fault, there is an increase in the peak of the amplitude and even more vibrations are observed in Fig. 16b.

3.4.1. Full oil condition

There was a significant rise in the value of GMF compared to the fundamental value that is 24 Hz. From Fig. 16b the GMF is 25.61 Hz and the peak of the amplitude is 0.5589 m/s^2 which shows a great increase when compared to all the previous cases. High quality gears are designed to transfer power by a combined sliding motion from one gear to the next as smoothly, quietly, and efficiently as possible. This means that the starting from the proper metal, the gear teeth are cut to precise dimensions about the geometric center. The tooth surfaces are ground smooth and any imperfections are removed. Each gear is properly fitted to a straight shaft to eliminate eccentricity. The shafts are spaced to optimize the tooth engagement. Any errors in gear manufacture or assembly and/or deterioration will result in a disturbance at gear mesh frequency with adjacent sidebands reflecting once per revolution modulation caused by pitch abnormalities in one or both gears. Since perfection is an asymptotic endeavour, gear systems always display some gear mesh action. Thus, the presence of the frequency is acceptable and should be apparent. The amplitude increases as the fault on the gearing increases.

3.4.2. Half oil condition

From Fig. 17b the GMF is noted as 22.58 and the peak amplitude is 0.5996 m/s^2, this shows some fluctuations in the GMF due to the fault and an increase

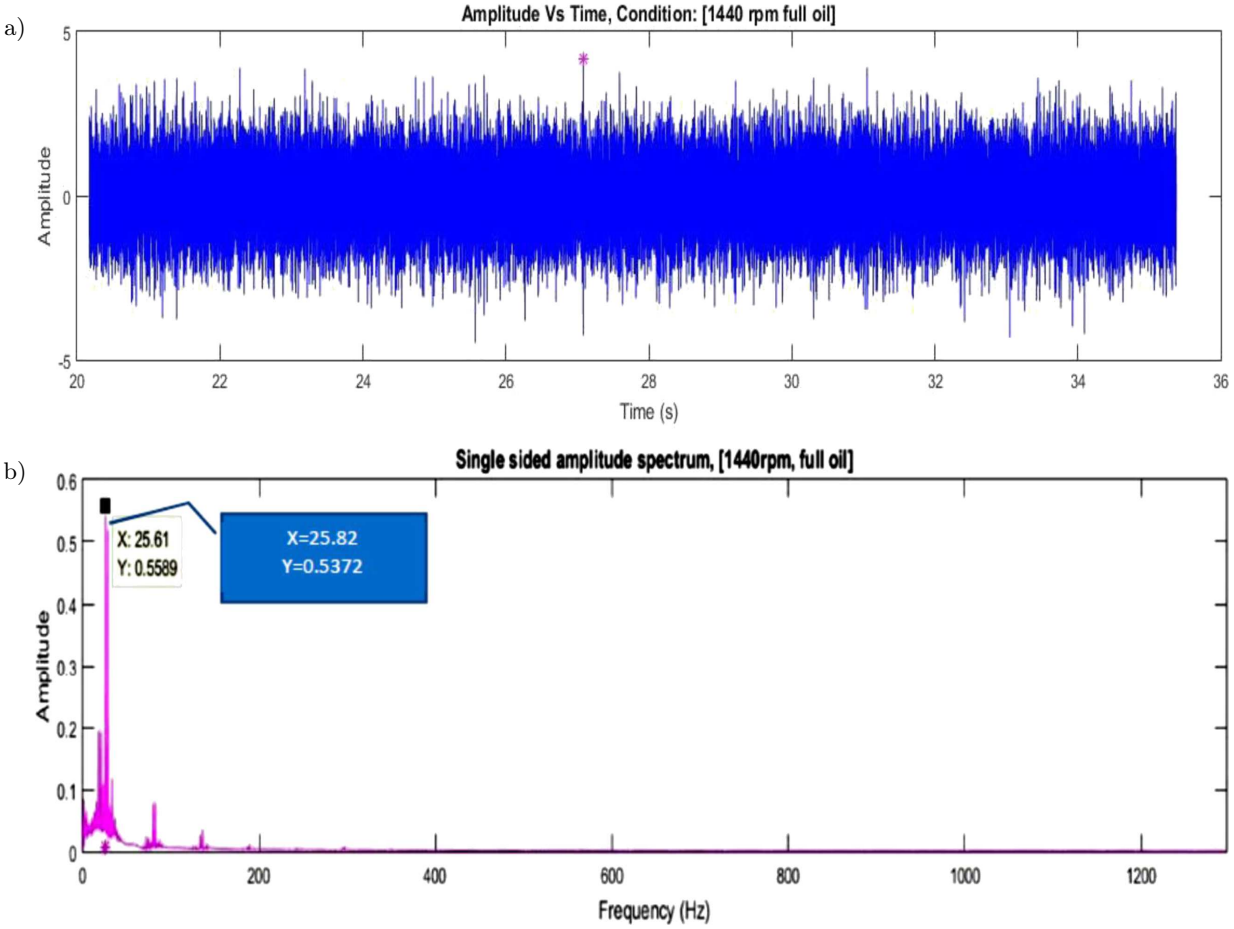

Fig. 16. a) Time domain signal for fault 3 under full oil condition, b) symlet decomposed signal through FFT for fault 3 under full oil condition.

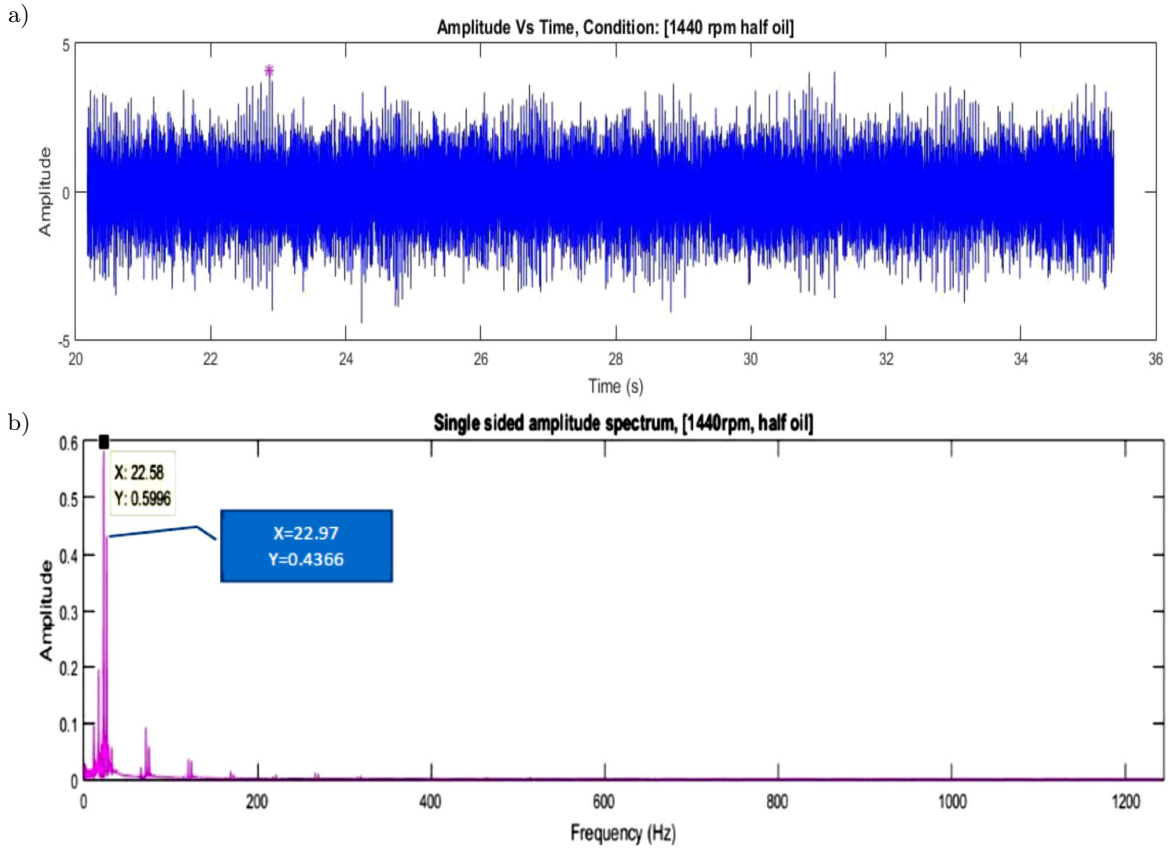

Fig. 17. a) Time domain signal for fault 3 under half oil condition, b) symlet decomposed signal through FFT for fault 3 under half oil condition.

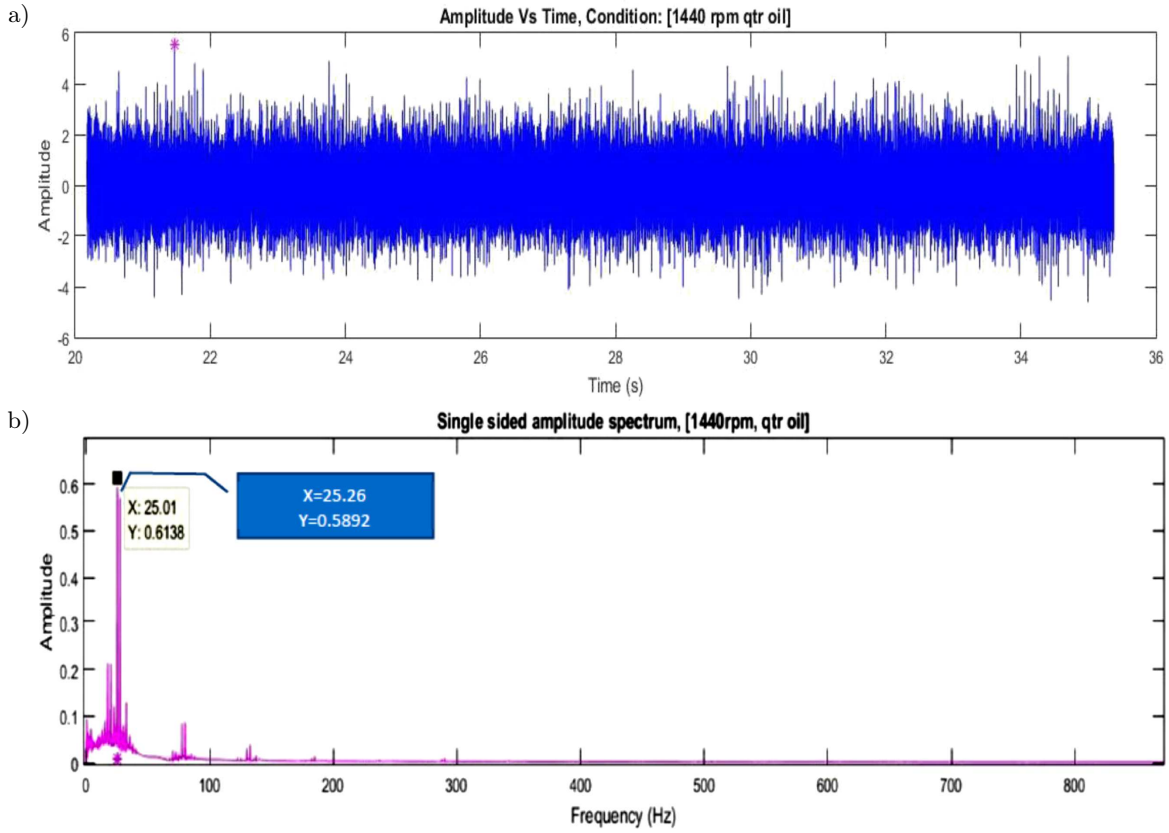

Fig. 18. a) Time domain signal for fault 3 under quarter oil condition, b) symlet decomposed signal through FFT for fault 3 under quarter oil condition.

in the amplitude since the oil level was reduced to half. A large increase in sideband amplitude suggests that there is a change in the geometry and is also a cause of fault. The relative amplitude of sideband to gear mesh peak is a good parameter and is observed from Fig. 17b.

3.4.3. Quarter oil condition

Corresponding to quarter oil condition, from Fig. 18b. the GMF was noted as 25.01 Hz and the peak amplitude as 0.6138 m/s^2. Thus, when compared to Fig. 7d, it is observed that there is a trend in increase in magnitude of vibration.

From Fig. 18b the relative amplitude of sideband to gear mesh peak is a good parameter to see in the plot. Scrutinize the waveform for periodic impacts that relate to rotational speed of the gears. The strong harmonics is developed and hence there is an indication of fault.

3.5. Worm gear box with fault 4

This fault corresponds to a condition where multiple faults were induced on the wheel. Further, the additional tooth was removed from the wheel using grinding machine. Also there is a trend in increase in the amplitude of vibration.

3.5.1. Full oil condition

As expected, with the increase in the magnitude of fault, a significant increase in the vibrational amplitude and fluctuations was noticed in the GMF, from Fig. 19b. GMF is 24.87 Hz and the peak amplitude is 0.7252 m/s^2 which shows a great increase in the amplitude. Analysing the sidebands is a very useful tool to characterize families of sidebands and modulation in a clear and easy way to interpret format as these become concentrated in harmonics which is shown in Fig. 19b.

3.5.2. Half oil condition

Corresponding to half oil condition, it is observed that there was an increase in the amplitude yet again proving that as the oil level reduces the peak amplitude increases. From Fig. 20b the GMF is 23.41 Hz and the peak amplitude is 0.7588 m/s^2. Sidebands are usually the result of an amplitude or frequency modulation process. In the spectrum, they take the form of spectral components equally spaced on both sides of the carrier frequency, symmetrically. The search for sidebands was only made around the components belonging to the identified harmonic series.

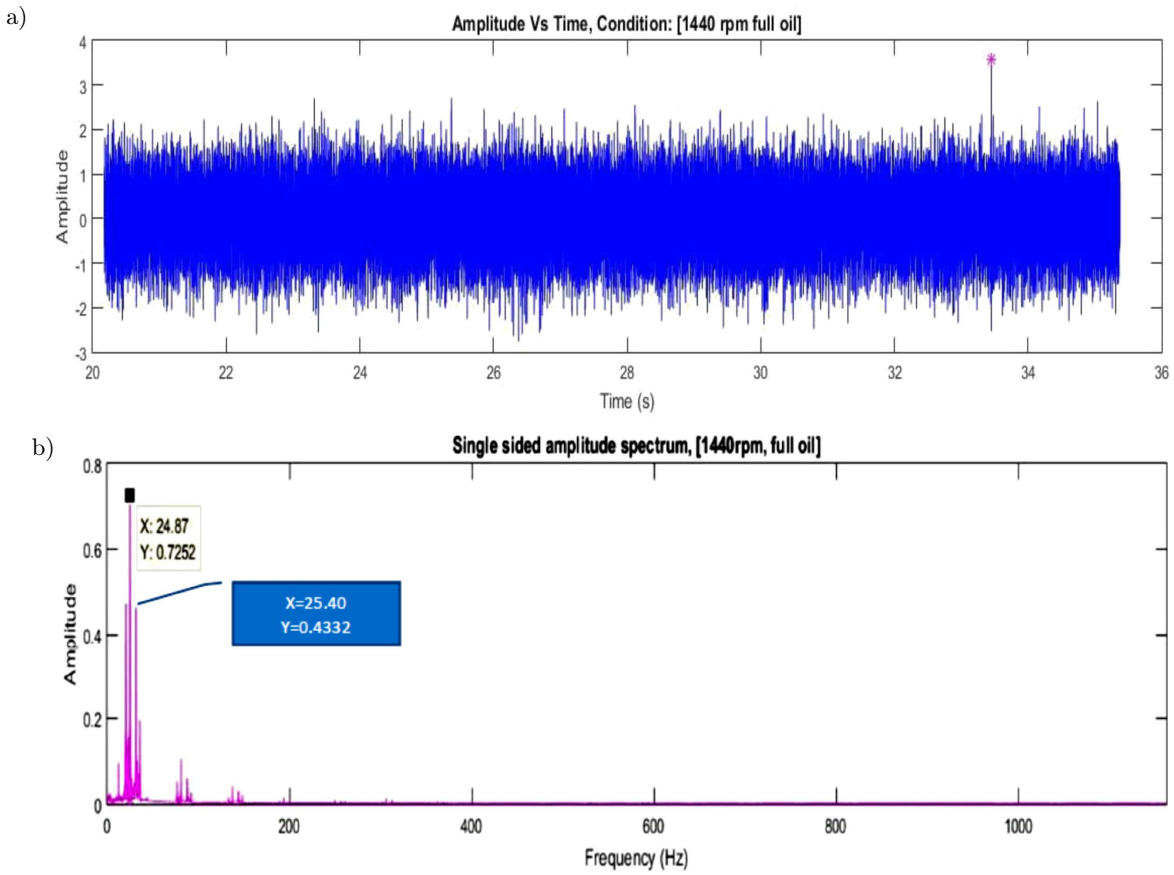

Fig. 19. a) Time domain signal for fault 4 under full oil condition, b) symlet decomposed signal through FFT for fault 4 under full oil condition.

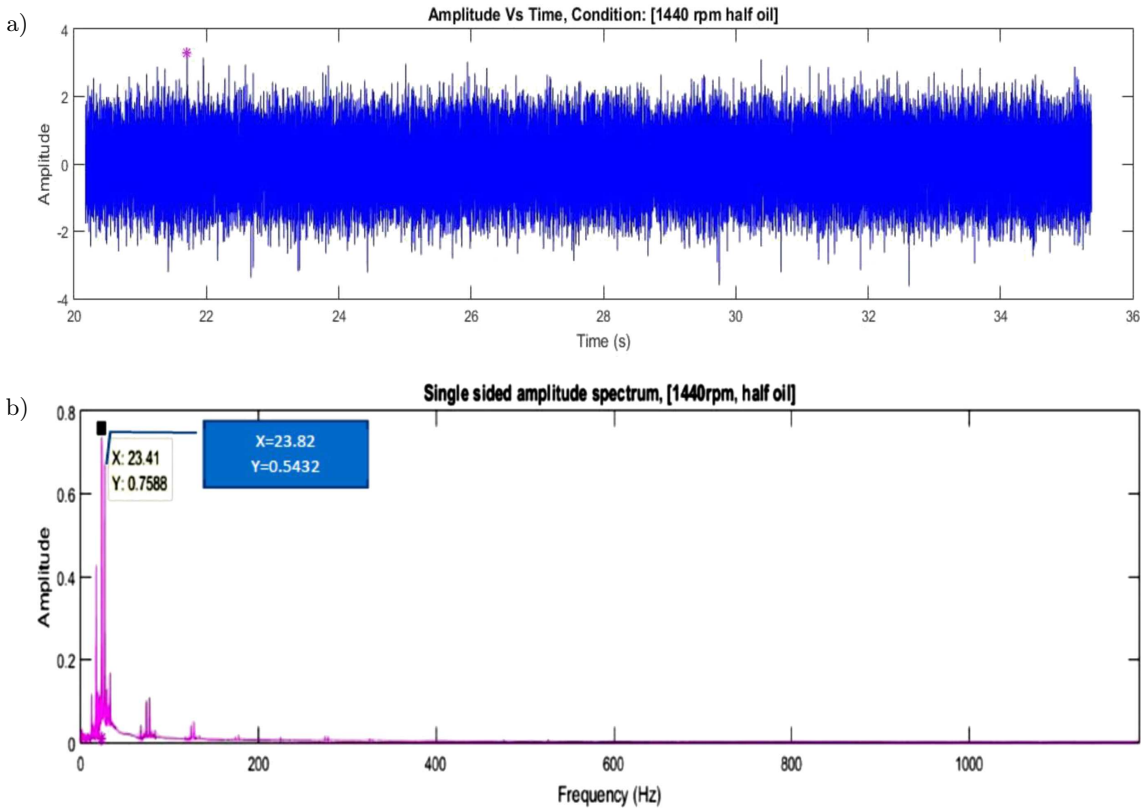

Fig. 20. a) Time domain signal for fault 4 under half oil condition, b) symlet decomposed signal through FFT for fault 4 under half oil condition.

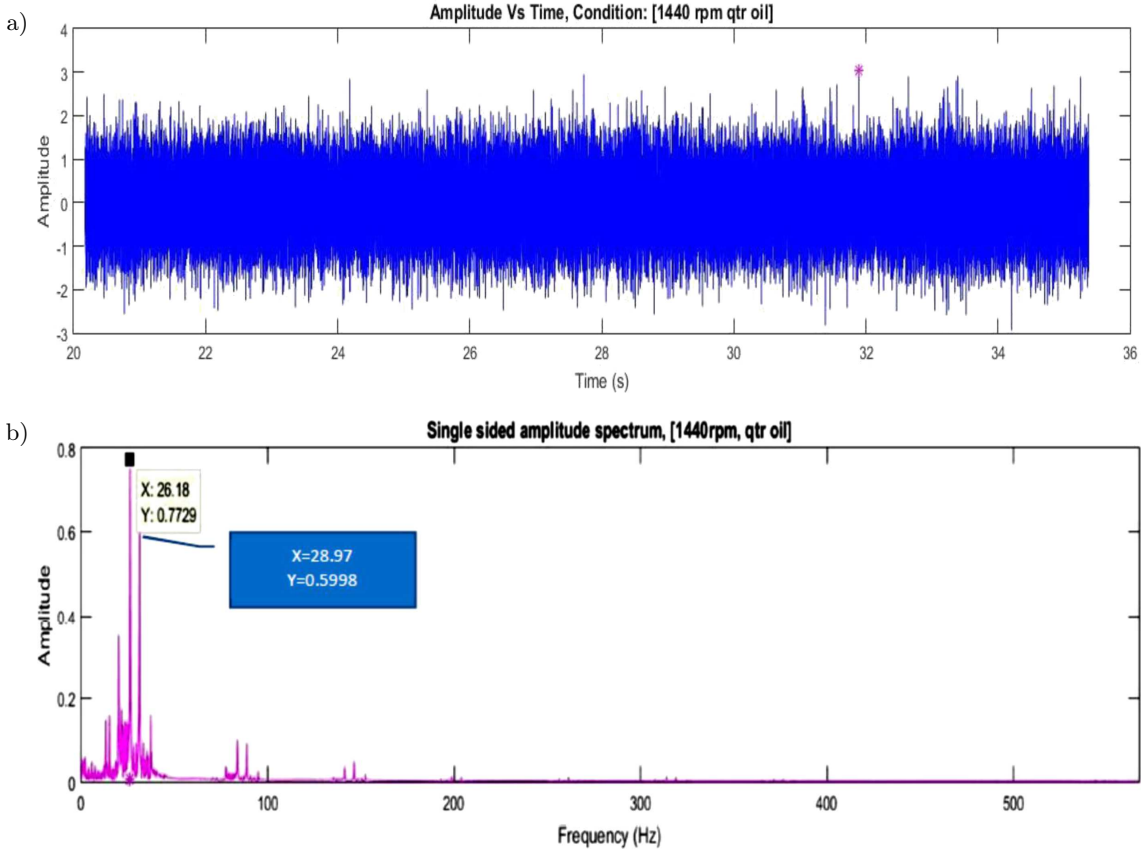

Fig. 21. a) Time domain signal for fault 4 under quarter oil condition, b) symlet decomposed signal through FFT for fault 4 under quarter oil condition.

3.5.3. Quarter oil condition

From Fig. 21b the GMF is 26.18 Hz which shows a great fluctuation from the fundamental value with a peak amplitude 0.7729 m/s^2. This shows that as the magnitude of fault increases the peak amplitude of vibration increases.

The symlet wavelet analysis is powerful in isolating peaks at sidebands of GMF which can provide more precise information about defect condition. Results show the vibration amplitude peak trend at GMF for different stages of fault from various power spectrums. FFT power spectrum shows minimum increase in vibration amplitude peak at GMF and symlet enveloped power spectrum shows considerable increase in comparison to other power spectrums. The proposed enveloped power spectrum technique is also applied for different oil level lubrication conditions. The proposed technique has less influence for the different fault conditions of the gear. The change in amplitude at GMF for different fault conditions is shown in Table 2. The gear mesh frequency and its harmonics are not expected to be suppressed; thus, the gear mesh frequency will have the highest amplitude with sidebands around it.

Table 2. Summary of results of Symlets wavelet decomposition for worm gear box.

Type of the gear box	Oil condition	Amplitude [m/s^2]	Frequency [Hz]
Healthy gear box	full oil	0.001893	24.07
	half oil	0.001937	25.54
	quarter oil	0.002559	25.55
Fault 1	full oil	0.1252	25.59
	half oil	0.1562	25.35
	quarter oil	0.1919	24.87
Fault 2	full oil	0.4245	25.09
	half oil	0.4607	25.23
	quarter oil	0.4931	24.57
Fault 3	full oil	0.5589	25.61
	half oil	0.5996	22.58
	quarter oil	0.6138	25.01
Fault 4	full oil	0.7252	24.87
	half oil	0.7588	23.41
	quarter oil	0.7729	26.18

From Table 2 one may observe a trend in the peak amplitude and it can also be seen that as the oil level decreases the amplitude of peak vibration increases and also as the magnitude of fault increases the peak amplitude also increases.

4. Artifical neural network

Figure 22 shows neural network used for automatic fault classification of gear. After giving an input of 30 samples with 9 features and a target matrix through excel and a target matrix of 30×5, the neural network started to train itself with the given data and shows the following outputs. This performance diagram shows the drops in network error. A cross entropy function was used for validating the data. The blue line shows error in the training data and the green line shows error in the validation data, training comes to an end when the error in the validation data is decreased whereas the red line shows error in the test data, thus the best validation error is observed at epoch 48 in Fig. 23.

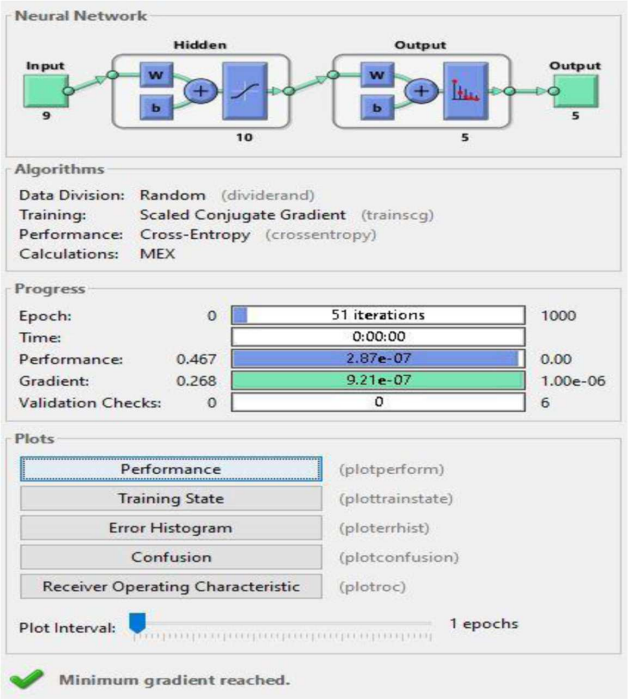

Fig. 22. Neural network.

This graph shows the number of times the validation failed for the given data. From Fig. 24 it is evident that the algorithm sees the data 19 times and a total of 6 validation checks are given.

The interpretation and performance of results are portrayed with the help of confusion matrix which shows validity of results (Fig. 25). It consists of four different matrices which are training matrix, validation matrix, testing matrix and all confusion matrix.

4.1. Training matrix

The samples that had been used to train these neural network were used to create this matrix. Each row indicates the predicted classification and the columns represents the correctly classified samples and similarly the diagonal cells corresponds to the samples which

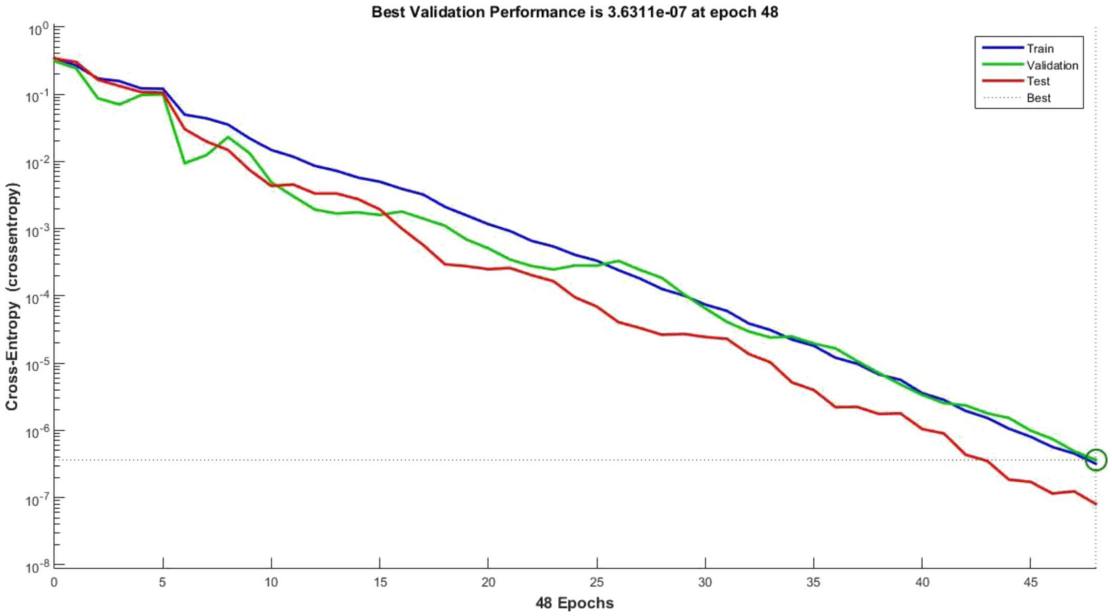

Fig. 23. Performance diagram.

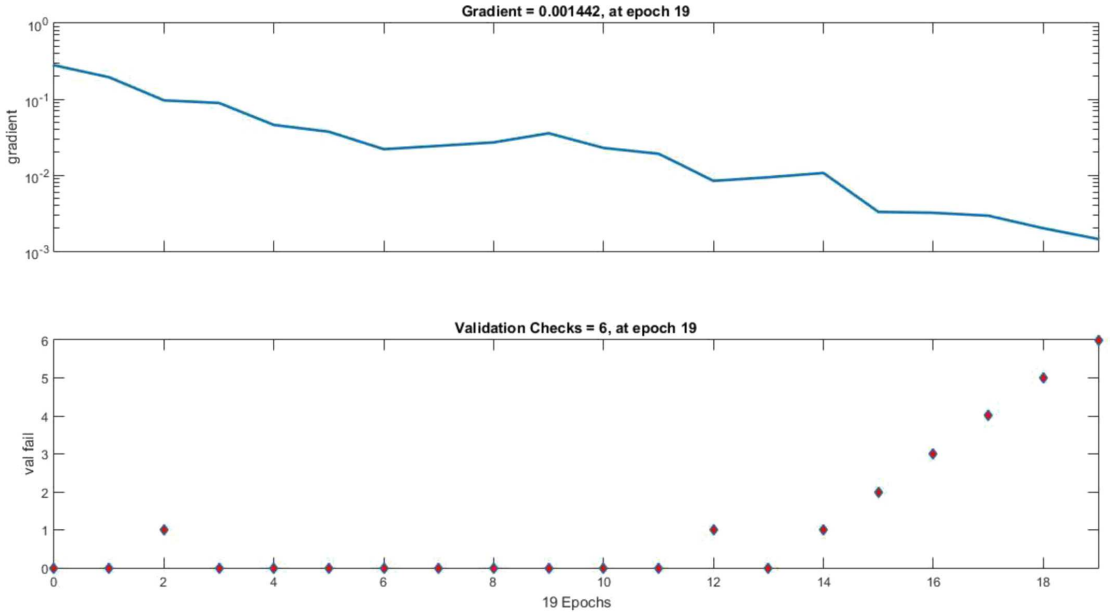

Fig. 24. Training performance.

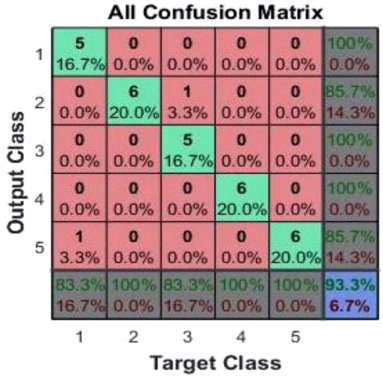

Fig. 25. Confusion matrix summary.

are correctly and precisely classified in classes. The column at the far right shows the percentage of all the sample predicted to belong to the correctly plus incorrectly classified classes. These are known as precise (+ve prediction rate) and rate of false discovery respectively. The bottom rows represent the percentage of all the samples that belong to the correctly plus incorrectly classified classes. These are known as recall (true positive rate) and false negative rate respectively. The most bottom point shows the overall accuracy of the training sample data. The result obtained has an accuracy of 94.7% for the training samples.

4.2. Validation matrix and testing matrix

As the name suggests the sample data that were used for validating the network were also used to generate this matrix. The rows indicate the predicted or the output class and columns indicate the true or the class of target. The diagonal cells correspond to the observations which have to be classified correctly and similarly the off diagonal cells correspond to the observations that are not correctly classified. The column at the far right side represents the percentage of all the samples predicted to belong to the correctly plus incorrectly classified classes. These are known as precise (+ve prediction rate) and false discovery rate respectively. The row at the deep bottom represents the percentage of all the samples that belong to the correctly plus incorrectly classified classes. These are known as recall (true +ve rate) and false negative rate respectively. The most bottom point shows the overall accuracy of the validation sample data. The result obtained had an accuracy of 100% for the validating sample. The result obtained had an accuracy of 80% for the testing matrix.

4.3. Confusion matrix

In this matrix the whole dataset is used to form the matrix. The rows indicate the predicted or the class of output and the columns indicate the true or the targeted class. The diagonal cells correspond to the observations that are correctly and precisely classified and similarly the off diagonal cells correspond to the observation that are not correctly classified. The column at the far right represents the percentage of all the samples predicted to belong to the correctly as well as incorrectly classified classes. These are known as precise (+ve prediction rate) and false discovery rate respectively. The bottom row represents the percentage of all samples which properly belong to the correctly, incorrectly classified classes. These are known as recall (true +ve rate) and false negative rate respectively. The most bottom point shows the overall accuracy of the results obtained. The result obtained had an accuracy of 93.3%.

Usually ROC depicts various things. From Fig. 26 the following conclusions can be drawn:

1) It tells us the trade-off between the sensitivity which is true positive rate and specificity or false

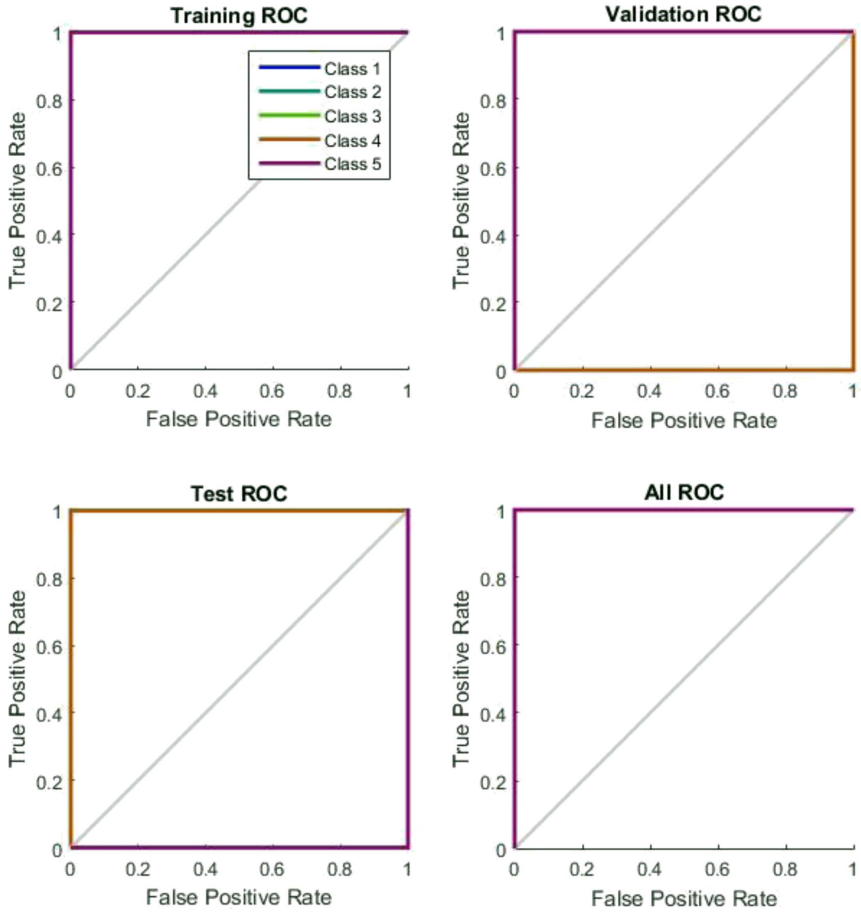

Fig. 26. ROC plots.

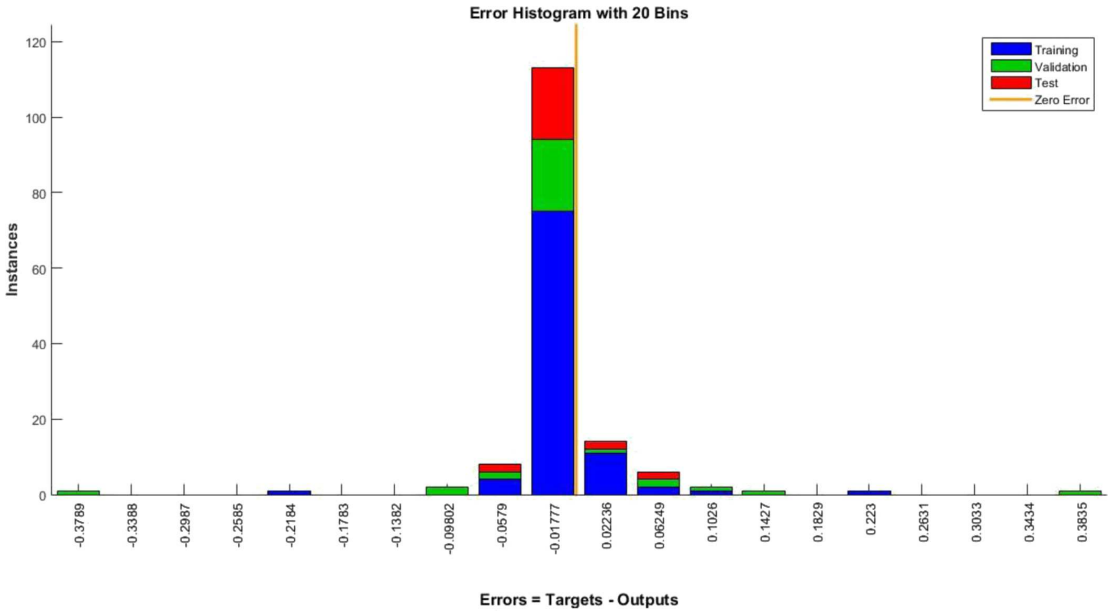

Fig. 27. Error histogram.

positive rate, i.e. as the sensitivity decreases the specificity increases.

2) When the curve comes closer to 45 degrees then the test becomes less accurate.
3) The area under the curve gives the test accuracy.

From the plot in Fig. 27 it can be said that it is a good result since the area under the true positive rate is big and it do not cross the false positive rate.

The error histogram with 20 bins represents the instances vs error graph. Error can be defined as

$$\text{Errors} = \text{Targets} - \text{Outputs}.$$

The data obtained from histogram shows that the values are near to zero and negative indicating inverse condition, thus we can validate the results by saying that when the values are near to 0 and 1, the network is highly accurate. In the plot the orange line indicates zero error, blue color indicates training sample, red is testing sample. and the green part is validation sample. The number of instances can be seen on the y axis.

5. Conclusions

In this study, the symlets wavelet was implemented and the vibration analysis on the worm gear box was conducted. The data show spikes in the amplitude as the fault magnitude increases, and also show the fluctuation of the gear mesh frequency due to the application of various faults. The symlet wavelet also proved to be effective in increasing the resolution of the signal without any loss of information and it also facilitates elimination of the additional vibrations caused by the motor and coupling. Hence, the symlet wavelet can be used to locate the exact fault on worm gear box and it gives the exact power spectrum density plot. This study also highlights the use of artificial neural networks using the npr tool in MATLAB Simulink. The statistical features like RMS, crest factor, shape factor etc., were used as the input data and the health of the gear box was used for output data. An overall accuracy of 93.3% was obtained using ANN. Vibration signal can be consistently measured and monitored to check the structural health condition of worm gear box which can help to reduce operating costs.

References

1. Antoniadou I., Manson G., Staszewski W.J., Barszcz T., Worden K. (2015), A time-frequency analysis approach for condition monitoring of a wind turbine gearbox under varying load conditions, *Mechanical Systems and Signal Processing*, **64–65**: 188–216, doi: 10.1016/j.ymssp.2015.03.003.

2. Elasha F., Ruiz-Cárcel C., Mba D., Kiat G., Nze I., Yebra G. (2014), Pitting detection in worm gearboxes with vibration analysis, *Engineering Failure Analysis*, **42**: 366–376, doi: 10.1016/j.engfailanal.2014.04.028.

3. Elforjani M., Mba D., Muhammad A., Sire A. (2012), Condition monitoring of worm gears, *Applied Acoustics*, **73**(8): 859–863, doi: 10.1016/j.apacoust.2012.03.008.

4. Fan X., Zuo M.J. (2006), Gearbox fault detection using Hilbert and wavelet packet transform, *Mechanical Systems and Signal Processing*, **20**(4): 966–982.

5. Ghodake S.B., Mishra A.K., Deokar A.V. (2016a), A review paper on fault detection of worm gearbox,

International Advanced Research Journal in Science, Engineering and Technology, **3**(1): 161–164.

6. Ghodake S.B., Mishra A.K., Deokar A.V. (2016b), Experimental analysis of faults in worm gearbox using vibration analysis, *International Engineering Research Journal*, **1**: 1518–1523, http://www.ierjournal.org/pupload/mitpgcon/1518-1523.pdf.

7. Ismon M.B., Zaman I.B., Ghazali M.I. (2015), Condition monitoring of variable speed worm gearbox lubricated with different viscosity oil, *Applied Mechanics and Materials*, **773–774**: 178–182, doi: 10.4028/www.scientific.net/AMM.773-774.178.

8. Jing L., Zhao M., Li P., Xu X. (2017), A convolutional neural network based feature learning and fault diagnosis method for the condition monitoring of gearbox, *Measurement*, **111**: 1–10, doi: 10.1016/j.measurement.2017.07.017.

9. Kalkat M. (2015), Investigations on the effect of oil quality on gearboxes using neural network predictors, *Industrial Lubrication and Tribology*, **67**(2): 99–109, doi: 10.1108/ilt-02-2013-0020.

10. Kumar R., Singh M. (2013), Outer race defect width measurement in taper roller bearing using discrete wavelet transform of vibration signal, *Measurement*, **46**(1): 537–545, doi: 10.1016/j.measurement.2012.08.012.

11. Li C., Liang M. (2012), Time-frequency signal analysis for gearbox fault diagnosis using a generalized synchrosqueezing transform, *Mechanical Systems and Signal Processing*, **26**: 205–217, doi: 10.1016/j.ymssp.2011.07.001.

12. Peng Z., Kessissoglou N. (2003), An integrated approach to fault diagnosis of machinery using wear debris and vibration analysis, *Wear*, **255**(7–12): 1221–1232, doi: 10.1016/S0043-1648(03)00098-X.

13. Rajput P., Kumar S. (2015), Development of novel denoising technique using total variation and symlet wavelet filter, *International Journal of Engineering Trends and Technology*, **22**(3): 109–114.

14. Singh A., Parey A. (2019), Gearbox fault diagnosis under non-stationary conditions with independent angular re-sampling technique applied to vibration and sound emission signals, *Applied Acoustics*, **144**: 11–22, doi: 10.1016/j.apacoust.2017.04.015.

15. Tilak T.N., Krishnakumar S. (2015), Effectiveness of symlets in de-noising fingerprint images, *International Journal of Computer Sciences and Engineering*, **3**(12): 29–34, http://www.ijcseonline.org/pub_paper/4-IJCSE-01410.pdf.

16. Wang W.J., McFadden P.D. (1996), Application of wavelets to gearbox vibration signals for fault detection, *Journal of Sound and Vibration*, **192**(5): 927–939, doi: 10.1006/jsvi.1996.0226.

17. Zhang Z-Y., Wang K-S. (2014), Wind turbine fault detection based on SCADA data analysis using ANN, *Advances in Manufacturing*, **2**(1): 70–78, doi: 10.1007/s40436-014-0061-6.